LZTR1 is a regulator of RAS ubiquitination and signaling

Johannes W. Bigenzahn[1], **Giovanna M. Collu**[2], **Felix Kartnig**[1], **Melanie Pieraks**[1], **Gregory I. Vladimer**[1], **Leonhard X. Heinz**[1], **Vitaly Sedlyarov**[1], **Fiorella Schischlik**[1], **Astrid Fauster**[1,3], **Manuele Rebsamen**[1], **Katja Parapatics**[1], **Vincent A. Blomen**[3], **André C. Müller**[1], **Georg E. Winter**[1], **Robert Kralovics**[1,4], **Thijn R. Brummelkamp**[1,3,5,6], **Marek Mlodzik**[2], **Giulio Superti-Furga**[1,7,*]

[1]CeMM Research Center for Molecular Medicine of the Austrian Academy of Sciences, 1090 Vienna, Austria [2]Department of Cell, Developmental, & Regenerative Biology and Graduate School of Biomedical Sciences, Icahn School of Medicine at Mount Sinai, 1 Gustave L. Levy Place, New York, NY 10029, USA [3]Netherlands Cancer Institute, Plesmanlaan 121, 1066 CX, Amsterdam, Netherlands [4]Department of Laboratory Medicine, Medical University of Vienna, 1090 Vienna, Austria [5]Oncode Institute, Division of Biochemistry, Netherlands Cancer Institute, Plesmanlaan 121, 1066 CX, Amsterdam, Netherlands [6]Cancer Genomics Center (CGC.nl), Plesmanlaan 121, 1066 CX, Amsterdam, Netherlands [7]Center for Physiology and Pharmacology, Medical University of Vienna, 1090 Vienna, Austria

Abstract

In genetic screens aimed at understanding drug resistance mechanisms in chronic myeloid leukemia cells, inactivation of the cullin 3 adapter protein-encoding leucine zipper like transcription regulator 1 (*LZTR1*) gene led to enhanced mitogen-activated protein kinase (MAPK) pathway activity and reduced sensitivity to tyrosine kinase inhibitors. Knockdown of the *Drosophila LZTR1* orthologue *CG3711* resulted in a RAS-dependent gain-of-function phenotype. Endogenous human LZTR1 associates with the main RAS isoforms. Inactivation of *LZTR1* led to decreased ubiquitination and enhanced plasma membrane localization of endogenous KRAS (V-Ki-ras2 Kirsten rat sarcoma viral oncogene homolog). We propose that LZTR1 acts as a conserved regulator of RAS ubiquitination and MAPK pathway activation. Because *LZTR1* disease mutations failed to revert loss-of-function phenotypes, our findings provide a molecular rationale for *LZTR1* involvement in a variety of inherited and acquired human disorders.

*Correspondence and requests for materials should be addressed to: Giulio Superti-Furga, CeMM Research Center for Molecular Medicine of the Austrian Academy of Sciences, Lazarettgasse 14, AKH BT25.3, 1090 Vienna, Austria; gsuperti@cemm.oeaw.ac.at; Telephone: +43 1 40160 70 001; Fax: +43 1 40160 970 000.

Chronic myeloid leukemia (CML) is characterized by the expression of the constitutively active oncogenic tyrosine kinase fusion BCR-ABL (1). The proliferation and survival of BCR-ABL^{+} CML cells depends on the activation state of key cellular signaling networks including the mitogen-activated protein kinase (MAPK) pathway (1). The development of the tyrosine kinase inhibitor (TKI) imatinib has provided a successful targeted therapeutic however limited by the development of resistance (2).

Genetic screens in the near-haploid human CML cell line KBM-7 allow unbiased identification of candidate genes affecting inhibitor resistance (3). We performed comprehensive haploid genetic screening with six TKIs in clinical use or under evaluation (Fig. S1A). Retroviral gene-trap mutagenized cells were exposed to the TKIs at concentrations corresponding to half maximal inhibitory concentration (IC^{50}) to IC^{70} dosage (Fig. S1B), resistant cell populations were collected after selection and genomic gene-trap insertions identified by deep sequencing. Each screen resulted in enrichment of disruptive insertions in 5 to 18 different genes (Fig. 1A, Fig. S1C-G, S2A, and Table S1). We identified a recurrent set (4 screens) of six genes (*NF1*, *WT1*, *PTPN1*, *PTPN12*, *LZTR1*, *BAP1*; "TOP6" set) (Fig. 1B) with overrepresentation of disruptive genomic gene-trap integrations strongly indicating a selective advantage upon drug treatment (Fig. S2B).

We used a lentiviral CRISPR/Cas9 multi-color competition assay (MCA)-based coculture system to evaluate gene-mediated drug resistance effects. *SpCas9* expressing KBM-7 (KBM-7[Cas9]) cells were infected with lentiviral single guide RNA (sgRNA) vectors co-expressing reporter fluorophores enabling tracing of knockout and control cell populations by flow cytometry in the same well (Fig. S3A). Mixed sg*Ren* (targeting *Renilla luciferase*) control cell populations expressing fluorescent proteins (GFP[+] or mCherry[+]) did not show any preferential outgrowth of resistant cells upon 14 days of TKI treatment (Fig. 1C and Fig. S3H). In contrast, KBM-7[Cas9] GFP^{+} cells harboring sgRNAs that target the TOP6 genes showed decreased amount of cognate protein (Fig. S3B-G) and demonstrated enhanced cell survival and outgrowth in the presence of imatinib (Fig. 1C) and rebastinib (Fig. S3H). Thus, we functionally validated the TOP 6 genes as important for drug action in *BCR-ABL[+]* CML cells.

Although *NF1*, *PTPN1* and *PTPN12* share the ability to modulate MAPK pathway activation and *WT1* as well as *BAP1* function through transcriptional regulation (Fig. S2C), we could not deduce any mechanistic explanation for the role of leucine zipper like transcription regulator 1 (*LZTR1*) in enhanced CML cell survival from the existing literature (4, 5). To exclude cell line-specific effects, we confirmed that loss of *LZTR1* expression induced resistance to imatinib and rebastinib in other CML cell lines (Fig. S4A-C). Although we identified significant *LZTR1* enrichment only in four of the genetic screens, KBM-7[Cas9] sg*LZTR1* cells exhibited various degrees of resistance against all tested BCR-ABL TKIs (Fig. S3I). We used a CRISPR/Cas9-based domain scanning strategy to test whether both N-terminal Kelch domains and C-terminal Broad-Complex, Tramtrack, and Bric a brac (BTB) and partial BACK domains are essential for the drug resistance phenotype (6–8). All protein domain-targeting sgRNAs showed efficient indel formation (Fig. S3J) and induced resistant outgrowth of targeted cell populations exposed to rebastinib, indicating that the entire protein is functionally required (Fig. S3K). To determine whether LZTR1 exerts its function

only in a CML specific context, we infected FLT3-ITD$^+$ acute myeloid leukemia (AML) MV4-11^{Cas9} cells with *LZTR1*-targeting sgRNAs (Fig. S4D). FLT3 inhibitor treatment led to outgrowth of resistant cells underlining a more general role for *LZTR1* in the drug response of hematopoietic cancers driven by different tyrosine kinases (Fig. S4E-G).

KBM-7^{Cas9} CML cells infected with distinct sgRNAs targeting *LZTR1* displayed enhanced phosphorylation of MAPK kinase 1 (MEK1) and -2 and extracellular signal-regulated kinase 1 (ERK1) and -2, indicative of augmented MAPK pathway activation (Fig. 2A). By contrast, global tyrosine phosphorylation, as well as phosphorylation of AKT (at S473 and T308), the protein kinase S6K1, ribosomal protein S6 and the direct BCR-ABL substrate signal transducer and activator of transcription 5 (STAT5) remained unchanged (Fig. S4 J and K). Additional CML (K-562 and LAMA-84) and AML (MV4-11) cell lines had similarly enhanced MAPK pathway activation under normal growth conditions as well as, in the case of CML cells, upon increasing concentration of imatinib treatment (Fig. 2A, Fig. S4 H and I, and Fig. S5A-C). *LZTR1* full-length cDNA complementation in K-562^{Cas9} sg*LZTR1* cells reverted both enhanced MEK and ERK phosphorylation as well as TKI resistance (Fig. 2B and C). Treatment of K-562^{Cas9} sg*LZTR1* cells with the clinically approved inhibitor of MEK1 and -2 trametinib reverted enhanced activation of ERK1 and -2 and pharmacologically counteracted the drug resistance phenotype (Fig. 2D and E). Furthermore, cDNA expression of constitutively active *Mek1*$^{D218, D222}$ (Mek1 DD) in K-562^{rtTA3} cells led to enhanced phosphorylation of ERK1 and -2 and reduced imatinib sensitivity (Fig. S6A and B). Activation of the MAPK pathway could also be inferred by the gene expression and transcription factor enrichment signature obtained with RNA sequencing experiments in KBM-7^{Cas9} sg*LZTR1* compared to sg*Ren* cells (Fig. S5D and E and Table S2). Altogether, the data established a causal role for enhanced MAPK pathway activation in the resistance of CML cells towards TKI therapy as elicited by loss of LZTR1 function.

As BTB domain-containing proteins serve as adaptor proteins for the cullin 3 (CUL3) E3 ubiquitin ligase complex enabling specific substrate recognition and ubiquitination (9), we tested whether loss of CUL3 expression could mimic the observed LZTR1 loss-of-function phenotype. Indeed, K-562^{Cas9} sg*CUL3* cells demonstrated enhanced MAPK pathway activation and, in contrast to sg*LZTR1* cells, increased phosphorylation of AKT (Fig. S4K). However, sgRNAs targeting *CUL3* had a pronounced antiproliferative effect both in KBM-7^{Cas9} and K-562^{Cas9} cells (Fig. S6C and D) therefore providing a potential explanation why *CUL3* was not detected in our genetic screens (Fig. S2A).

In contrast to the CML cell lines, depletion of LZTR1 with CRISPR sgRNAs in HeLa, human embryonic kidney (HEK)-293T or HAP1 cells did not increase MAPK pathway activation under comparable culture conditions (Fig. S7A and C). However, after serum stimulation of cells cultured without serum, HEK293T^{Cas9} sg*LZTR1* cells showed a more pronounced activation of MEK and ERK than in control cells (Fig. S7B). Similarly, in HAP1 cells, a non-hematopoietic derivative of the KBM-7 cell line (10), phorbol-12-myristat-13-acetat (PMA) treatment led to enhanced MAPK pathway activation in the absence of *LZTR1* compared with that in wild-type (WT) cells (Fig. S7C). Whereas HAP1^{Cas9} sg*CUL3* cells exhibited increased phosphorylation of ERK1, ERK2 and AKT (Fig. S7F), loss of *LZTR1*

expression in HAP1^{Cas9} altered only the MAPK pathway as identified by means of pathway array-based assessment of kinase activation (Fig. S7D-E and Table S3).

Genetic studies have identified *LZTR1* mutations in glioblastoma (GBM) (11), schwannomatosis (SWNMT) (8) and Noonan syndrome (NS) (5), a developmental syndrome which is part of the larger group of RASopathies characterized by mutations in components of the RAS-MAPK pathway (12). Identification of *NF1* and *LZTR1* loss-of-function-induced MAPK pathway activation in our haploid resistance screens combined with human *LZTR1* mutations in NS indicated that LZTR1 might directly regulate guanosine triphosphatases (GTPases) of the RAS family.

Drosophila wing vein formation and eye development serve as excellent *in vivo* readouts for RAS signaling (13–15). *CG3711* encodes the *Drosophila* orthologue of mammalian *LZTR1*, which contains a unique N-terminal domain (amino acids 1-184) that is only found in *Drosophila*. This is followed by the highly conserved remaining part of the protein (54% sequence identity) (Fig. S8A-C). Systemic depletion of *CG3711* with RNA interference using *act5C-Gal4* yielded viable flies; however, the majority of wings of these flies displayed wing vein defects characterized by extra veins and vein tissue (Fig. 3A and B and Fig. S8D). This phenotype closely resembles a gain-of-function increase of RAS-MAPK signaling (15) and could be rescued by a decrease in abundance of RAS via *dRas* (*Drosophila* Ras) heterozygosity (Fig. 3C). *Drosophila* R7 photoreceptor induction requires RAS function (13, 14). We used a mild dominant negative version, Ras$^{V12\,C40}$, which although locked in the active 5′-triphosphate (GTP)-bound state does not activate MAPK signaling (16). Ras$^{V12\,C40}$ expression in the developing eyes (via the *sevenless/sev-Gal4* expression system) led to a frequent loss of the R7 photoreceptor (~30% of ommatidia display R7 loss, and some also lost other R-cells) (Fig. S8E and H). Because Ras$^{V12\,C40}$ is constitutively active, it also causes defects in ommatidial rotation (16, 17), serving as internal control. When both *sev-Gal4* driven *CG3711* RNAi and Ras$^{V12\,C40}$ were expressed, the loss of R7 phenotype was almost completely suppressed (Fig. S8F and H). The ommatidial rotation defects were enhanced rather than suppressed because these involve MAPK-independent RAS signaling (16) (Fig. S8F). Expression of *CG3711* RNAi in the eye alone did not induce phenotypic changes (Fig. S8G and H). Thus, RAS is crucial for the phenotypes induced by depletion of *CG3711*.

To explore possible interactions of LZTR1 with RAS, we used a BirA* fusion protein-based proximity biotinylation-dependent (BioID) proteomic approach, which allows identification of weak interaction partners. We expressed KRAS4A, KRAS4B, NRAS and HRAS as N-terminal FLAG-BirA* fusion proteins in K-562^{rtTA3} CML cells. This led to enhanced MEK and ERK activation demonstrating that the BirA* tag does not generally interfere with RAS signaling (Fig. S9A). We identified between 153 and 258 proteins in proximity of or interacting with human RAS proteins, among them several known interactors and pathway components (Fig. S9B-F and Table S4). A common set of 123 proteins repeatedly purified with all four RAS proteins, with gene ontology analysis showing a significant enrichment in components associated with plasma membrane and Golgi apparatus as well as the MAPK pathway (Fig. S9G-H). We identified LZTR1 among the most significant interactors of all four RAS proteins (Fig. S9B-F). Intersection of the 123 common interactors identified by

BioID with a fluorescence-activated cell sorting (FACS)-based haploid genetic pathway screen for the identification of gene knockout alleles influencing phosphorylation of ERK1 and -2 (18) revealed LZTR1 as the only common RAS interactor in our proteomic data with a negative regulatory function within the RAS-MAPK pathway (Fig. S10A).

BioID proximity biotinylation-based and FLAG tag-based co-immunoprecipitation experiments confirmed the interaction of all four RAS proteins with endogenous LZTR1 (Fig. S10B and C). Only the four main RAS isoforms interacted specifically with LZTR1, whereas six related RAS family GTPases showed no interaction (Fig. S11A). Nine other canonical positive RAS-MAPK pathway regulators also failed to interact with endogenous LZTR1 (Fig. S11B). Immunoprecipitations with extracts derived from *LZTR1* knockout cells confirmed the specificity of the interaction (Fig. S11C). The C-terminal post-translational acylations of KRAS proteins appeared to be required for the interaction with LZTR1 (Fig. 3D and Fig. S11D). Thus, proper membrane associated localization mediated by this region may be required for specific interaction with LZTR1.

Stably expressed full-length hemagglutinin (HA)-tagged LZTR1 protein showed a speckled and vesicular staining pattern in HeLa, HEK293T and HAP1 cells whereas all domain mutants had a homogenous cytoplasmic distribution (Fig. S12A-D). Full-length LZTR1 displayed an overlapping localization within speckled and vesicular compartments with transiently transfected V5-tagged CUL3 in HeLa cells (Fig. S13A). The LZTR1-stained speckles further overlapped with the autophagosome marker LC3B fused to mCherry (Fig. S13B), but we failed to detect LZTR1 localization with marker proteins of the Golgi, lysosome, peroxisome or early and late endosome compartments (Fig. S13C). Isoform-specific antibodies that recognize endogenous human RAS isoforms are not available (19). We therefore endogenously tagged KRAS (Fig. S14A), and confirmed specificity of detection in immunofluorescence and immunoblotting by genetic inactivation of the tagged genomic allele (Fig. S14 B to D). KRAS localized to a large number of small-punctate structures, likely membrane-containing small vesicles (Fig. 3E and Fig. S14D). Inactivation of endogenous *LZTR1* led to an increased RAS signal, particularly at the periphery of cells, at regions of cell-to-cell contacts (Fig. 3E and Fig. S14D). This phenotype appeared to be dependent on the CUL3 E3 ligase complex, because genetic inactivation of *CUL3* led to similar phenotypic changes (Fig. 3E and Fig. S14E).

We also assessed interaction of endogenously tagged KRAS with exogenous LZTR1 in HAP1 cells (Fig. S15A). Exogenous LZTR1 localized to fewer, larger, and more oblong structures than endogenous KRAS (Fig. S15B). A fraction of the LZTR1-stained structures also contained KRAS. Treatment with the cullin neddylation inhibitor MLN4924 caused clustering of LZTR1-containing structures that appeared to surround particles strongly stained with KRAS (Fig. S15B, MLN4924 panel). Caution is required for the interpretation of these patterns because LZTR1 was overexpressed, and KRAS was at endogenous concentration. However, the images could represent a trapped proteostatic process involving the two proteins.

We tested whether LZTR1 affected ubiquitination of RAS proteins by acting as a substrate adaptor for the CUL3 E3 ligase complex (11, 20). Ubiquitination of RAS proteins is known,

but little is known of its consequences (21–25). Co-expression of HA-ubiquitin with either one of the four RAS isoforms alone only resulted in a basal state of ubiquitination, but addition of MYC-tagged CUL3 and V5-tagged LZTR1 led to increased ubiquitination of RAS proteins (Fig. S16A-D). LZTR1-deletion mutants that lack either one or both C-terminal BTB domains or the N-terminal Kelch domain failed to induce an equivalent degree of ubiquitination of KRAS4A (Fig. S16A). KRAS4A required the presence of its C-terminal hypervariable (HVR) and the farnesylated cysteine 186 for LZTR1-mediated ubiquitination (Fig. S16E). LZTR1-induced ubiquitination was unchanged in cells treated with a proteasome inhibitor but could be blocked by cullin neddylation inhibition, which is consistent with the observed subcellular localization changes (Fig. S16F). Specificity for LZTR1 in the process was further underscored by the failure of two prominent CUL3 adaptors, Kelch-like ECH-associated protein 1 (KEAP1) and Speckle-type POZ protein (SPOP), to cause a comparable ubiquitination (Fig. S16G). We used HAP1 cells bearing endogenously tagged KRAS and tandem ubiquitin binding domain (TUBE) reagents, to capture endogenously ubiquitinated proteins and evaluate the contribution of endogenous LZTR1 (26). In the absence of any stimulation, immunoprecipitation with TUBE purified several proteins that reacted with pan-ubiquitin antibodies (Fig. 3F, third panel from the top, and Fig. S16H). The same precipitates contained proteins reacting with pan-RAS antibodies (Fig. 3F, second panel from the top). Last, FLAG antibodies detected a protein not visible in the whole cell extract (Fig. 3F, first panel from the top, and Fig. S16H). TUBE-mediated immunoprecipitation from corresponding cells in which LZTR1 had been genetically inactivated did not contain amounts of RAS detectable with these antibodies (Fig. 3F, first and second panel from the top, and Fig. S16H). The signal obtained with pan-ubiquitin antibodies was unchanged (Fig. 3F, third panel from the top, and Fig. S16H). Thus, human LZTR1 appears to mediate ubiquitination of endogenous human KRAS and possibly other RAS proteins.

If a main function of LZTR1 is to regulate RAS, then loss of RAS function should compensate for loss of LZTR1 activity as suggested in the fruit fly epistatic analysis, thereby representing an ideal experimental setup to assess the disease-associated *LZTR1* mutations by their dependency on RAS activity. We confirmed that loss of LZTR1 function enhanced RAS activity in K-562 cells (Fig. S17A). We then performed CRISPR/Cas9-based double knockout MCA experiments (Fig. S17B-D). Single sg*LZTR1* and sg*LZTR1*-sg*Ren* double-infected cells were resistant to imatinib compared to control sg*Ren* cells (Fig. S17E-F). sgRNAs targeting *KRAS* abolished cellular outgrowth, whereas sgRNAs targeting *NRAS*, *HRAS* and *RIT1* failed to do so (Fig. S17E-F). sg*LZTR1*-sg*KRAS* cells had reduced MEK phosphorylation comparable to that of sg*Ren* cells, whereas sg*NRAS* and sg*HRAS* cells maintained enhanced MAPK pathway activation (Fig. S17G). *KRAS* inactivation led to a strong antiproliferative phenotype in KBM-7^{Cas9} cells and, to a lesser extent, K-562^{Cas9} cells (Fig. S18 A and B), indicating that the selective requirement of *KRAS* in mediating *LZTR1*-induced enhanced MAPK pathway activation might represent a prerequisite of *KRAS* for BCR-ABL signaling in CML cells. We additionally used a fibronectin-fold-based monobody, NS1, which bears low nanomolar affinity for the dimerization interface of both KRAS and HRAS, and is able to interfere with their signaling activities (27). Cells stably

expressing the NS1 monobody did not show increased activation of the MAPK pathway or drug resistance associated with loss of LZTR1 function (Fig. S18 C and D).

More than 50 different mutations have been mapped to the human *LZTR1* gene in various diseases (5, 28) (8, 11, 29, 30) (Fig. S19A-B and Table S5). To establish a mechanistic link between mutations that affect human diseases and the biochemical processes described here, we focused on *LZTR1* missense mutations identified in GBM (11), NS (5) and SWNMT (8) (Fig. S20B). Mutation-bearing *LZTR1* cDNAs were tested for their ability to complement K-562 CML cells deficient in endogenous *LZTR1* (Fig. S20A). In contrast to WT LZTR1, the disease-associated mutations failed to reduce MAPK pathway activation, despite being expressed at comparable or higher amount (Fig. 4A-C). Similarly, all missense mutations apart from the GBM-associated T288I and R810W failed to restore sensitivity to imatinib treatment (Fig. S20C-E). LZTR1 mutations within the Kelch domain partially retained their localization pattern in comparison to the WT protein, whereas mutations in the BTB/BACK domains mislocalized to the cytoplasm (Fig. S21 A and B). In agreement, expression of LZTR1 Kelch domain mutations identified in GBM, NS and SWNMT in K-562 WT cells had a resistance-mediating effect in MCA assays in cells treated with imatinib, whereas BTB/BACK domain mutations did not (Fig. S22A-C). Furthermore, in contrast to the LZTR1 WT protein, the two mutants R198G and G248R identified in GBM and NS failed to induce a similar increase in ubiquitination on KRAS4A (Fig. S22D). These findings provide functional evidence that human LZTR1 missense mutations identified in GBM, NS and SWNMT represent loss-of-function towards ubiquitination and inhibition of RAS activity.

Together with the accompanying manuscript on the role of LZTR1 in diseases driven by the dysregulation of RAS ubiquitination and signaling (Steklov, Pandolfi, Baietti et al. SCIENCE 2018) our work illustrates the importance of an additional, underappreciated layer of RAS regulation (Fig. 4D).

Supplementary Material

Refer to Web version on PubMed Central for supplementary material.

Acknowledgments

References

1. Ren R. Mechanisms of BCR–ABL in the pathogenesis of chronic myelogenous leukaemia. Nat Rev Cancer. 2005; 5:172–183. [PubMed: 15719031]

2. O'Hare T, Zabriskie MS, Eiring AM, Deininger MW. Pushing the limits of targeted therapy in chronic myeloid leukaemia. Nat Rev Cancer. 2012; 12:513–526. [PubMed: 22825216]

3. Carette JE, et al. Global gene disruption in human cells to assign genes to phenotypes by deep sequencing. Nature Biotechnology. 2011; 29:1–7.

4. Simanshu DK, Nissley DV, McCormick F. RAS Proteins and Their Regulators in Human Disease. Cell. 2017; 170:17–33. [PubMed: 28666118]

5. Yamamoto GL, et al. Rare variants in SOS2 and LZTR1 are associated with Noonan syndrome. J Med Genet. 2015; 52:413–421. [PubMed: 25795793]

6. Canning P, et al. Structural basis for Cul3 protein assembly with the BTB-Kelch family of E3 ubiquitin ligases. J Biol Chem. 2013; 288:7803–7814. [PubMed: 23349464]

7. Nacak TG, Leptien K, Fellner D, Augustin HG, Kroll J. The BTB-kelch protein LZTR-1 is a novel Golgi protein that is degraded upon induction of apoptosis. J Biol Chem. 2006; 281:5065–5071. [PubMed: 16356934]

8. Piotrowski A, et al. Germline loss-of-function mutations in LZTR1 predispose to an inherited disorder of multiple schwannomas. Nat Genet. 2014; 46:182–187. [PubMed: 24362817]

9. Xu L, et al. BTB proteins are substrate-specific adaptors in an SCF-like modular ubiquitin ligase containing CUL-3. Nature. 2003; 425:316–321. [PubMed: 13679922]

10. Carette JE, et al. Ebola virus entry requires the cholesterol transporter Niemann-Pick C1. Nature. 2011; 477:340–343. [PubMed: 21866103]

11. Frattini V, et al. The integrated landscape of driver genomic alterations in glioblastoma. Nat Genet. 2013; 45:1141–1149. [PubMed: 23917401]

12. Tidyman WE, Rauen KA. The RASopathies: developmental syndromes of Ras/MAPK pathway dysregulation. Curr Opin Genet Dev. 2009; 19:230–236. [PubMed: 19467855]

13. Therrien M, et al. KSR, a novel protein kinase required for RAS signal transduction. Cell. 1995; 83:879–888. [PubMed: 8521512]

14. Karim FD, et al. A screen for genes that function downstream of Ras1 during Drosophila eye development. Genetics. 1996; 143:315–329. [PubMed: 8722784]

15. Oishi K, et al. Phosphatase-defective LEOPARD syndrome mutations in PTPN11 gene have gain-of-function effects during Drosophila development. Hum Mol Genet. 2009; 18:193–201. [PubMed: 18849586]

16. Gaengel K, Mlodzik M. Egfr signaling regulates ommatidial rotation and cell motility in the Drosophila eye via MAPK/Pnt signaling and the Ras effector Canoe/AF6. Development. 2003; 130:5413–5423. [PubMed: 14507782]

17. Brown KE, Freeman M. Egfr signalling defines a protective function for ommatidial orientation in the Drosophila eye. Development. 2003; 130:5401–5412. [PubMed: 14507785]

18. Brockmann M, et al. Genetic wiring maps of single-cell protein states reveal an off-switch for GPCR signalling. Nature. 2017; 546:307–311. [PubMed: 28562590]

19. Waters AM, et al. Evaluation of the selectivity and sensitivity of isoform- and mutation-specific RAS antibodies. Sci Signal. 2017; 10:eaao3332. [PubMed: 28951536]

20. Bennett EJ, Rush J, Gygi SP, Harper JW. Dynamics of cullin-RING ubiquitin ligase network revealed by systematic quantitative proteomics. Cell. 2010; 143:951–965. [PubMed: 21145461]

21. Jura N, Scotto-Lavino E, Sobczyk A, Bar-Sagi D. Differential modification of Ras proteins by ubiquitination. Molecular Cell. 2006; 21:679–687. [PubMed: 16507365]

22. Yan H, Jahanshahi M, Horvath EA, Liu H-Y, Pfleger CM. Rabex-5 ubiquitin ligase activity restricts Ras signaling to establish pathway homeostasis in Drosophila. Curr Biol. 2010; 20:1378–1382. [PubMed: 20655224]

23. Sasaki AT, et al. Ubiquitination of K-Ras enhances activation and facilitates binding to select downstream effectors. Sci Signal. 2011; 4:ra13. [PubMed: 21386094]

24. Baker R, et al. Differences in the regulation of K-Ras and H-Ras isoforms by monoubiquitination. J Biol Chem. 2013; 288:36856–36862. [PubMed: 24247240]

25. Rose CM, et al. Highly Multiplexed Quantitative Mass Spectrometry Analysis of Ubiquitylomes. Cell Syst. 2016; 3:395–403.e4. [PubMed: 27667366]

26. Hjerpe R, et al. Efficient protection and isolation of ubiquitylated proteins using tandem ubiquitin-binding entities. EMBO Rep. 2009; 10:1250–1258. [PubMed: 19798103]

27. Spencer-Smith R, et al. Inhibition of RAS function through targeting an allosteric regulatory site. Nat Chem Biol. 2017; 13:62–68. [PubMed: 27820802]

28. Johnston JJ, et al. Autosomal recessive Noonan syndrome associated with biallelic LZTR1 variants. Genet Med. 2018; doi: 10.1038/gim.2017.249

29. Gröbner SN, et al. The landscape of genomic alterations across childhood cancers. Nature. 2018; 555:321–327. [PubMed: 29489754]

30. Cancer Genome Atlas Research Network. Electronic address: wheeler@bcm.edu, Cancer Genome Atlas Research Network. Saksena G. Comprehensive and Integrative Genomic Characterization of Hepatocellular Carcinoma. Cell. 2017; 169:1327–1341.e23. [PubMed: 28622513]

31. Sanjana NE, Shalem O, Zhang F. Improved vectors and genome-wide libraries for CRISPR screening. Nat Methods. 2014; 11:783–784. [PubMed: 25075903]

32. Shalem O, et al. Genome-scale CRISPR-Cas9 knockout screening in human cells. Science. 2014; 343:84–87. [PubMed: 24336571]

33. Montague TG, Cruz JM, Gagnon JA, Church GM, Valen E. CHOPCHOP: a CRISPR/Cas9 and TALEN web tool for genome editing. Nucleic Acids Research. 2014; 42:W401–7. [PubMed: 24861617]

34. Doench JG, et al. Rational design of highly active sgRNAs for CRISPR-Cas9-mediated gene inactivation. Nature Biotechnology. 2014; 32:1262–1267.

35. Lackner DH, et al. A generic strategy for CRISPR-Cas9-mediated gene tagging. Nat Commun. 2015; 6:10237. [PubMed: 26674669]

36. Lampson BL, et al. Rare codons regulate KRas oncogenesis. Curr Biol. 2013; 23:70–75. [PubMed: 23246410]

37. Bigenzahn JW, et al. An Inducible Retroviral Expression System for Tandem Affinity Purification Mass-Spectrometry-Based Proteomics Identifies Mixed Lineage Kinase Domain-like Protein (MLKL) as an Heat Shock Protein 90 (HSP90) Client. Mol Cell Proteomics. 2016; 15:1139–1150. [PubMed: 26933192]

38. Dull T, et al. A third-generation lentivirus vector with a conditional packaging system. J Virol. 1998; 72:8463–8471. [PubMed: 9765382]

39. Schambach A, et al. Lentiviral vectors pseudotyped with murine ecotropic envelope: increased biosafety and convenience in preclinical research. Exp Hematol. 2006; 34:588–592. [PubMed: 16647564]

40. Fellmann C, et al. An optimized microRNA backbone for effective single-copy RNAi. Cell Rep. 2013; 5:1704–1713. [PubMed: 24332856]

41. Couzens AL, et al. Protein interaction network of the mammalian Hippo pathway reveals mechanisms of kinase-phosphatase interactions. Sci Signal. 2013; 6:rs15. [PubMed: 24255178]

42. Sakuma T, Nakade S, Sakane Y, Suzuki K-IT, Yamamoto T. MMEJ-assisted gene knock-in using TALENs and CRISPR-Cas9 with the PITCh systems. Nat Protoc. 2016; 11:118–133. [PubMed: 26678082]

43. Jae LT, et al. Virus entry. Lassa virus entry requires a trigger-induced receptor switch. Science. 2014; 344:1506–1510. [PubMed: 24970085]

44. Krzywinski M, et al. Circos: an information aesthetic for comparative genomics. Genome Res. 2009; 19:1639–1645. [PubMed: 19541911]

45. Brinkman EK, Chen T, Amendola M, van Steensel B. Easy quantitative assessment of genome editing by sequence trace decomposition. Nucleic Acids Research. 2014; 42:e168. [PubMed: 25300484]

46. Schindelin J, et al. Fiji: an open-source platform for biological-image analysis. Nat Methods. 2012; 9:676–682. [PubMed: 22743772]

47. Rappsilber J, Ishihama Y, Mann M. Stop and go extraction tips for matrix-assisted laser desorption/ionization, nanoelectrospray, and LC/MS sample pretreatment in proteomics. Anal Chem. 2003; 75:663–670. [PubMed: 12585499]

48. Olsen JV, et al. Parts per million mass accuracy on an Orbitrap mass spectrometer via lock mass injection into a C-trap. Mol Cell Proteomics. 2005; 4:2010–2021. [PubMed: 16249172]

49. Kersey P, Hermjakob H, Apweiler R. VARSPLIC: alternatively-spliced protein sequences derived from SWISS-PROT and TrEMBL. Bioinformatics. 2000; 16:1048–1049. [PubMed: 11159319]

50. Colinge J, Masselot A, Giron M, Dessingy T, Magnin J. OLAV: towards high-throughput tandem mass spectrometry data identification. Proteomics. 2003; 3:1454–1463. [PubMed: 12923771]

51. Teo G, et al. SAINTexpress: improvements and additional features in Significance Analysis of INTeractome software. J Proteomics. 2014; 100:37–43. [PubMed: 24513533]

52. Mellacheruvu D, et al. The CRAPome: a contaminant repository for affinity purification-mass spectrometry data. Nat Methods. 2013; 10:730–736. [PubMed: 23921808]

53. R Core Team. R: A Language and Environment for Statistical Computing. 2016. (available at https://www.R-project.org)

54. Heberle H, Meirelles GV, da Silva FR, Telles GP, Minghim R. InteractiVenn: a web-based tool for the analysis of sets through Venn diagrams. BMC Bioinformatics. 2015; 16:169. [PubMed: 25994840]

55. Huang DW, Sherman BT, Lempicki RA. Systematic and integrative analysis of large gene lists using DAVID bioinformatics resources. Nat Protoc. 2009; 4:44–57. [PubMed: 19131956]

56. Tomlinson A, Bowtell DD, Hafen E, Rubin GM. Localization of the sevenless protein, a putative receptor for positional information, in the eye imaginal disc of Drosophila. Cell. 1987; 51:143–150. [PubMed: 3115593]

57. Love MI, Huber W, Anders S. Moderated estimation of fold change and dispersion for RNA-seq data with DESeq2. Genome Biol. 2014; 15:550. [PubMed: 25516281]

58. Marbach D, et al. Tissue-specific regulatory circuits reveal variable modular perturbations across complex diseases. Nat Methods. 2016; 13:366–370. [PubMed: 26950747]

One Sentence Summary

Genetic screens for BCR-ABL TKI resistance identify *LZTR1* as mediator of RAS ubiquitination and regulator of MAPK pathway activation.
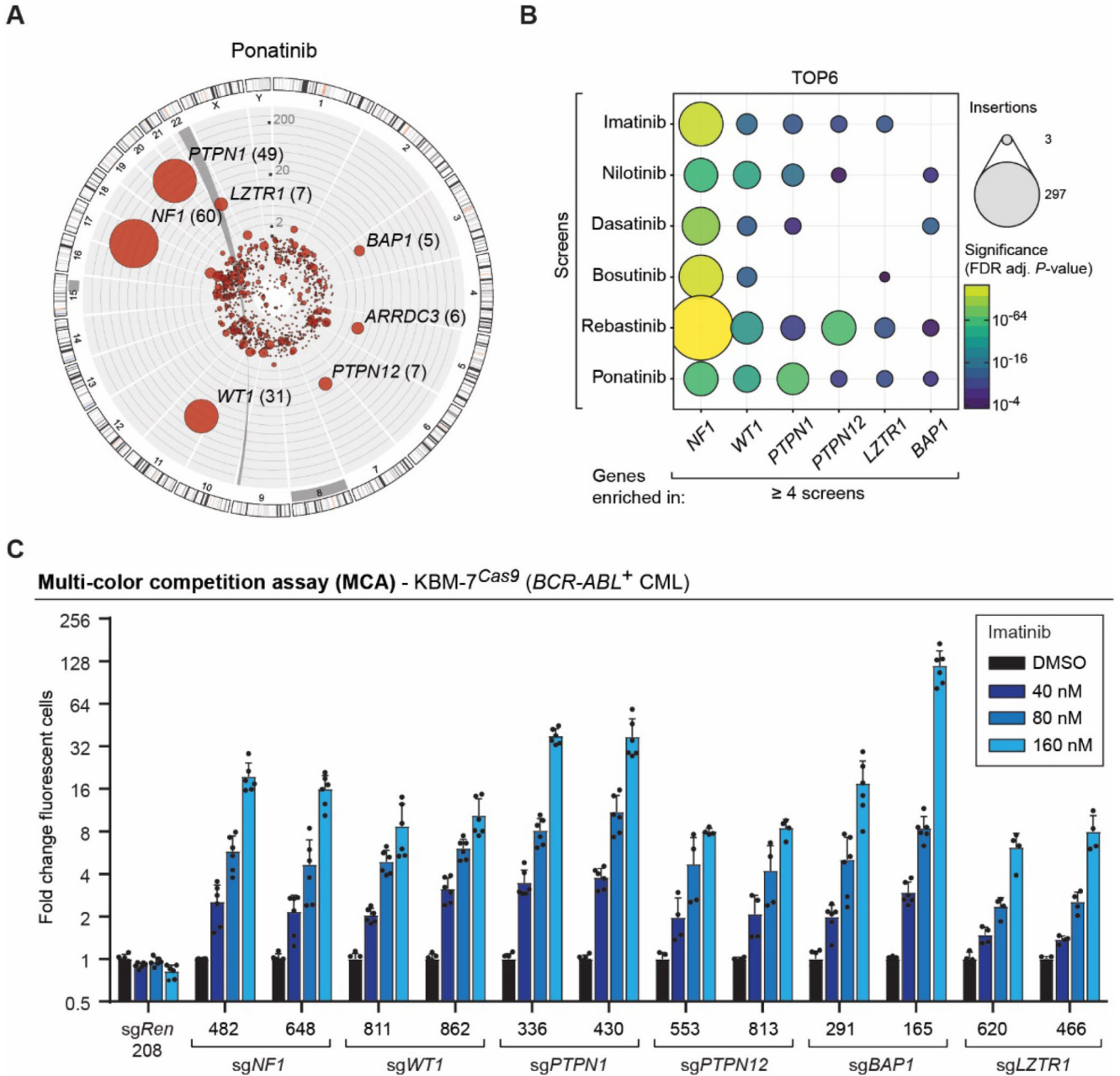
Figure 1. Haploid genetic screens identify gene knockouts promoting BCR-ABL inhibitor resistance.

(**A**) Circos plot of the haploid genetic screen in the CML cell line KBM-7 upon treatment with ponatinib. Each dot represents a mutagenized gene identified in the resistant cell population, the dot size corresponds to the number of independent insertions identified per gene and the distance from the circos plot center indicates the significance of enrichment compared to an unselected control data set. Hits with a false discovery rate (FDR) adjusted *P*-value lower than 10^{-4} are labeled by gene name. (**B**) Bubble plot depicting the "TOP6" set of genes identified in four or more of the six haploid screens upon treatment with 1st, 2nd and 3rd generation BCR-ABL inhibitors. The size of each bubble corresponds to the number

of independent insertions per gene and the color gradient depicts the FDR adjusted *P*-value of enrichment significance. **(C)** Multi-color competition assay (MCA)-derived fold change of cell populations after imatinib treatment of KBM-7^{Cas9} CML cells transduced with sgRNAs targeting the "TOP6" genes or sg*Ren*.208 (targeting *Renilla luciferase*) as negative control. sgRNA-infected cell populations were mixed in a 1:1 ratio, treated with increasing drug concentrations and analyzed by flow cytometry after 14 days. Data are shown as mean value ± s.d. of at least two independent experiments (n ≥ 2) performed in duplicates. sgRNAs are labeled by gene name followed by the genomic targeting sequence position numbered according to the sequence position on the corresponding mRNA.
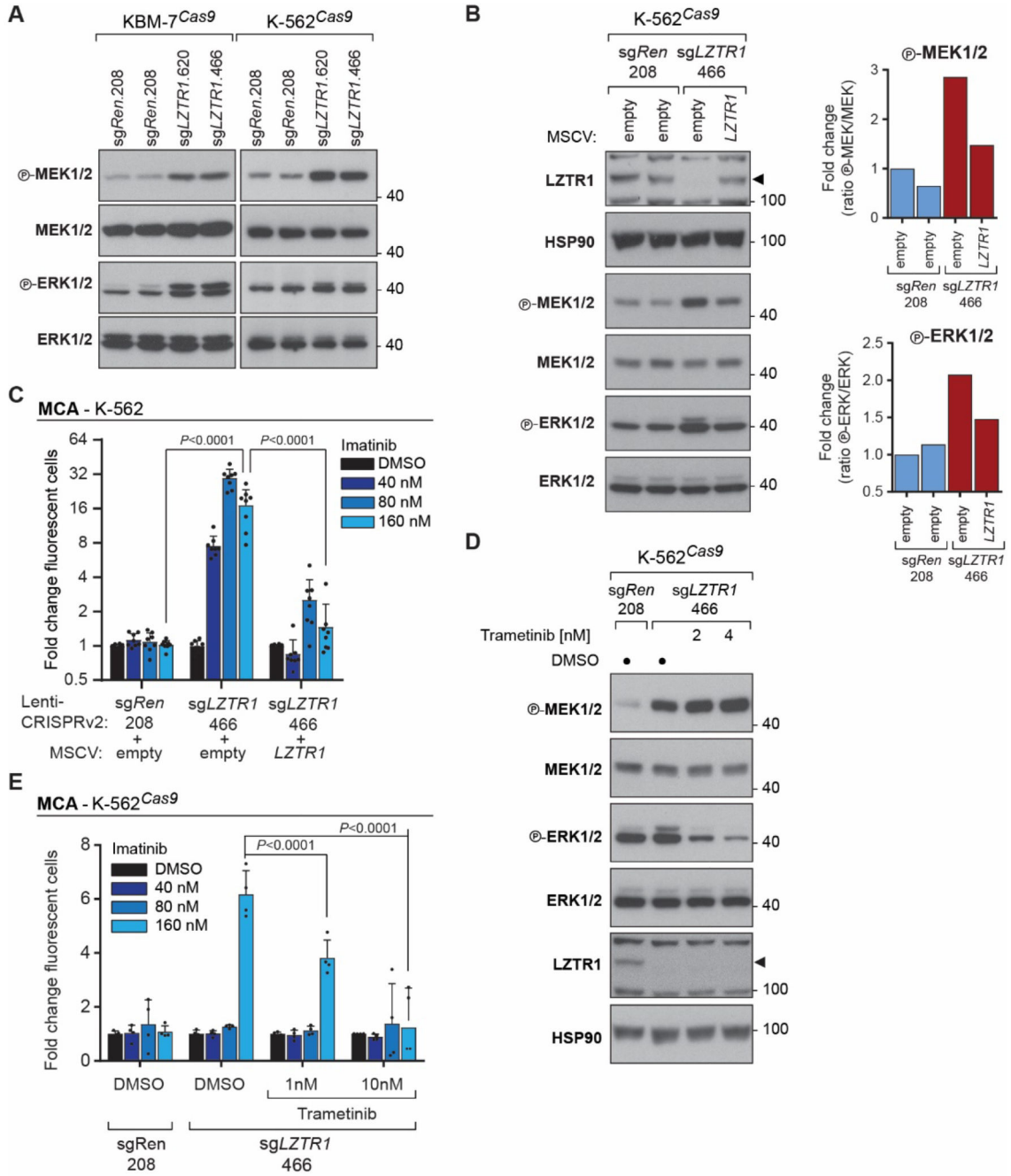
Figure 2. Loss of *LZTR1* enhances MAPK pathway activation.
(**A**) Phosphorylation of MEK and ERK in KBM-7^{Cas9} and K-562^{Cas9} CML cells transduced with the indicated sgRNAs. (**B**) Immunoblot analysis of MEK and ERK phosphorylation as well as LZTR1 expression in sg*Ren*.208-expressing K-562^{Cas9} CML cells transduced with empty vector, and sg*LZTR1*.466-expressing cells transduced with empty vector or *LZTR1*-cDNA-containing MSCV retrovirus. Quantification of MEK and ERK phosphorylation is shown next to the corresponding immunoblots. (**C**) Competitive proliferation assay (MCA) of K-562^{Cas9} sg*Ren*.208 cells transduced with empty vector and sg*LZTR1*.466 cells

transduced with empty vector or *LZTR1* cDNA after treatment with increasing concentrations of imatinib for 14 days. **(D)** Phosphorylation of MEK and ERK in K-562^{Cas9} cells expressing sg*LZTR1*.466 and treated with increasing concentrations of trametinib for 3 hours. **(E)** Changes in cell populations measured by MCA of K-562^{Cas9} CML cells expressing sg*Ren*.208 or sg*LZTR1*.466 after 14 days of treatment with increasing concentrations of imatinib alone or in combination with trametinib. Immunoblot results in **(A, B and D)** are representative of at least two independent biological experiments (n 2). MCA data in **(C, E)** are shown as mean value ± s.d. of at least two independent experiments (n 2). DMSO treatment served as negative control.
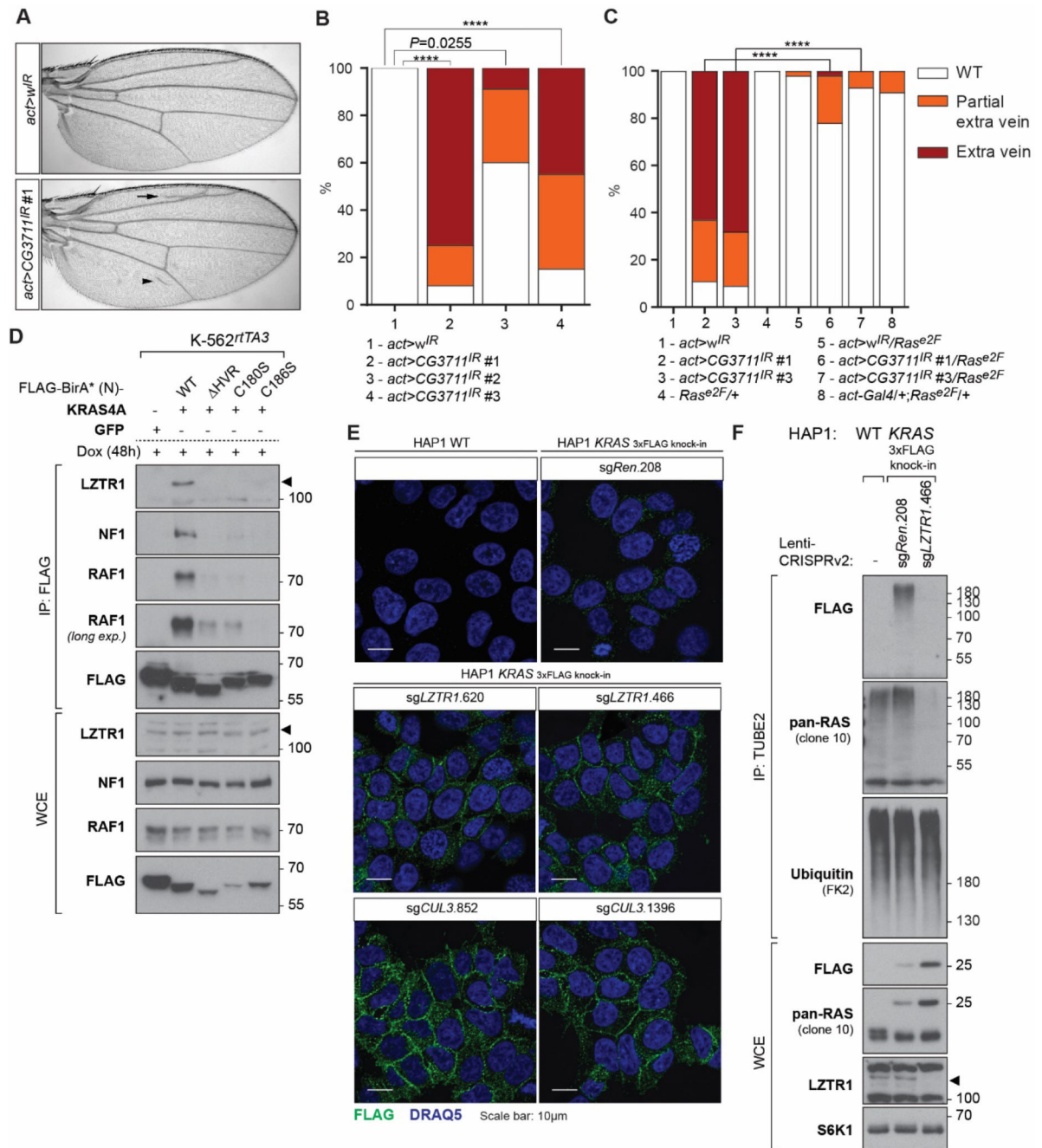
Figure 3. LZTR1 modulates MAPK pathway activation through RAS regulation.
(**A**) Morphology of adult wings from *act5C-Gal4, UAS-w^{IR}* (*act>w^{IR}* for short) and
act>CG3711^{IR} #1 RNAi fly lines. (**B**) Quantification of *act>w^{IR}* and *act>CG3711^{IR}* RNAi
lines as percentage of wings with ectopic wing vein formation. *P*-value for RNAi #1 and #3
in the wing is <0.0001 (****) and for #2 is 0.0255. (**C**) Quantification of *act>w^{IR}* and
act>CG3711^{IR} RNAi lines alone or in a *Ras^{e2F}/+* background as percentage of wings with
ectopic wing vein formation. For statistical assessment, partial extra vein and extra vein
formation have been combined. *P*-value for both RNAi line comparisons in the wing is

<0.0001 (****). **(D)** FLAG immunoprecipitates (IP) and whole cell extracts (WCE) from K-562^{rtTA3} cells expressing FLAG-BirA* tagged GFP or KRAS4A WT, HVR, C180S or C186S after 48 hours of doxycycline treatment were immunoblotted for the indicated proteins. **(E)** Confocal microscopy of HAP1 WT cells and HAP1 cells with endogenously FLAG-tagged KRAS transduced with sg*Ren*.208, sg*LZTR1*.620, sg*LZTR1*.466, sg*CUL3*.852 or sg*CUL3*.1396 and stained with anti-FLAG. Scale bar in all panels is 10μm. **(G)** Tandem ubiquitin binding domain (TUBE)-based purifications of ubiquitinated proteins and whole cell extracts (WCE) from HAP1 WT and endogenously FLAG-tagged KRAS cells transduced with sg*Ren*.208 or sg*LZTR1*.466 were analyzed by immunoblotting with the indicated antibodies. WT, wild type.
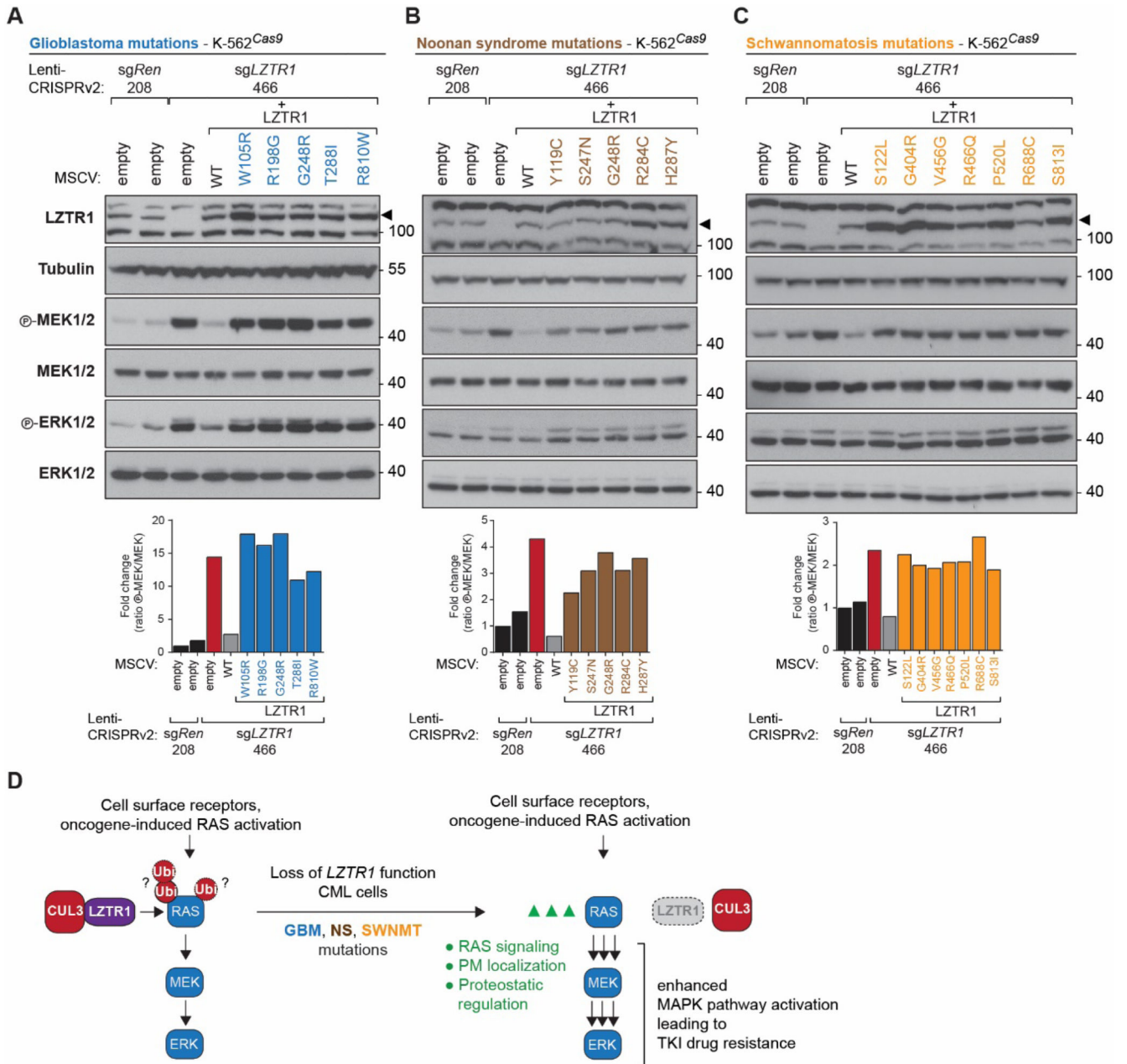
Figure 4. *LZTR1* disease missense mutations fail to rescue the loss-of-function phenotype.
(A-C) Immunoblotting for MEK and ERK phosphorylation as well as LZTR1 expression of
K-562^{Cas9} sg*Ren*.208-expressing cells retrovirally transduced with empty vector, and
sg*LZTR1*.466-expressing cells transduced with either empty vector, LZTR1 WT, or LZTR1
mutations identified in GBM (blue) **(A)**, NS (brown) **(B)**, or SWNMT (orange) **(C)**. The
LZTR1 G248R mutation has been identified in both GBM and NS. Immunoblot results are
representative of at least two independent biological experiments (n   2) and quantification
of MEK phosphorylation in the displayed blots is shown. **(D)** Mechanistic model of CUL3-

LZTR1-mediated RAS ubiquitination and enhanced MAPK pathway activation and BCR-ABL inhibitor drug resistance induced by loss of *LZTR1* function.